Open Veterinary Journal, (2025), Vol. 15(1): 198-210
ISSN: 2226-4485 (Print)
ISSN: 2218-6050 (Online)
Research Article
DOI: *10.5455/OVJ.2025.v15.i1.19*

Submitted: 17/09/2024 Accepted: 20/11/2024 Published: 31/01/2025

Efficacy of a gelatin-based hemostatic sponge and hydroxyapatite–chitosan nanocomposites (nHAp/CS) on regeneration of radial bone defects in rabbits

Taher Naser Elmeshreghi[1]*, Fathy D. El-Seddawy[2], Mohamed Gomaa[2], Shimaa A. Ezzeldein[2] and Mustafa Abd El Raouf[2]

[1]*Department of Surgery and Theriogenology, Faculty of Veterinary Medicine, University of Tripoli, Tripoli, Libya*
[2]*Department of Surgery, Anesthesiology and Radiology, Faculty of Veterinary Medicine, Zagazig University, Zagazig, Egypt*

ABSTRACT

Background: Bone-graft substitutes are a frequently employed method for the clinical reconstruction of osseous bone defects, and research on synthetic biomaterials is currently ongoing. Absorbable hemostatic gelatin sponge and hydroxyapatite–chitosan nanocomposites (nHAp/CS) have gained popularity in recent years because of their inherent characteristics: osteogenesis, osteoconductivity, osteoinductivity, biodegradability, and biocompatibility.

Aim: The aim of the study was to evaluate the effectiveness of 1) a gelatin-based hemostatic sponge (Surgispon) and 2) a combination of a weight ratio of 75/25 nHAp/CS composite with a Surgispon for osteogenic potential in the treatment of full-thickness segmental osseous defects in the radius of rabbits.

Methods: The 18 New Zealand rabbits had 10-mm-induced segmental diaphyseal defects of the left limb radius and were randomly allocated into three groups: group I left the defects untreated (control group), group II used a Surgispon, and group III had a weight ratio of 75/25 nHAp/CS composite wrapped with a Surgispon. Quantitative evaluation of the bone repair at the defect site in each group (n = 6), radiographic, gross, computed tomography (CT), and histopathological examinations were performed at 6 weeks (n = 3) and 12 weeks (n = 3) postoperatively.

Results: The quantitative statistical analysis of various evaluation methods at 6 weeks post-implantation demonstrated that there was no statistically significant difference between the groups ($p > 0.05$). The statistically significant differences ($p < 0.05$) between groups I and II, while groups I and III, were evident 12 weeks postoperatively.

Conclusion: The findings of the radiographic, macroscopic, CT, and histopathological analyses firmly demonstrate that the combination of a 75/25 weight ratio composite of nHAp/CS with Surgispon is more effective than Surgispon alone in its ability to significantly increase bone formation. This could provide a prospective option for treating segmental bone defects.

Keywords: Absorbable hemostatic gelatin sponge, Hydroxyapatite–chitosan nanocomposites, Radial bone defects, Bone regeneration, Bone-graft substitutes.

Introduction

Bone has an intrinsic ability to regenerate in response to trauma, promote skeletal development, and undergo lifelong remodeling (Dimitriou *et al*., 2011). Segmental bone defects are incapable of spontaneous healing due to several causes, including excision of a bone tumor, infections, avascular necrosis, acquired and congenital limb deformities, high-energy trauma, and nonunion. The most common surgical procedure for segmental bone defects is bone grafting, which can be done using autologous grafts, allografts, or synthetic biomaterials. There are many other treatments available, such as distraction osteogenesis, the Masquelet technique, amputation, and endoprosthesis. However, these techniques necessitate technical expertise and are associated with a high rate of complications (Wang and Yeung, 2017; Laubach *et al*., 2023).

Bone autografts are widely regarded as the benchmark, but the availability of suitable bone tissue for autologous grafting is often limited, and the process of harvesting it is frequently associated with negative health outcomes for the recipient (Miron, 2024). Thus, finding effective bone substitutes is of utmost importance. Alloplastic grafts, also known as synthetic biomaterials, can be created using various chemical compositions such as metals, ceramics, polymers, and composites (Salamanca *et al*., 2023).

Synthetic biomaterials, such as gelatin, considered an attractive natural biopolymer, are produced by the hydrolysis of insoluble collagen (Kuttappan

***Corresponding Author:** Taher Naser Elmeshreghi. Department of Surgery and Theriogenology, Faculty of Veterinary Medicine, University of Tripoli, Tripoli, Libya. Email: *elmeshreghi.taher@gmail.com*

et al., 2016). A gelatin-based hemostatic sponge produced from bovine or porcine skin is available under the Surgifoam, Spongostan, Surgispon, and Gelfoam trademarks in a variety of forms and sizes (Sagar *et al*., 2022). Absorbable hemostatic gelatin sponge has gained significant recognition as efficacious scaffold within the discipline of bone tissue engineering due to their multiple beneficial aspects: biocompatibility, biodegradability, osteoinductivity, and osteoconductivity. Furthermore, these products are easily accessible in the marketplace, priced affordably, and devoid of any detrimental reactions (Paganelli *et al*., 2006; Rohanizadeh *et al*., 2008).

Hydroxyapatite (HAp) is commonly utilized in bone grafting due to its biocompatibility, osseointegration, nontoxicity, biodegradability, and good osteoconductive and osteoinductive qualities (Jo *et al*., 2017; Yu *et al*., 2017; Lei *et al*., 2019, 2020; Jyoti *et al*., 2021). It has been broadly acknowledged as the biomaterial of choice for bone substitutes owing to its exceptional chemical composition and crystallographic resemblance to the structure of human bone (Georgeanu *et al*., 2023). Chitosan (CS) is regarded as the second-most prevalent natural biopolymer after cellulose. It has the ability to promote cellular adhesion, proliferation, differentiation, and biocompatibility due to its structural similarity to glycosaminoglycan, an essential component of the extracellular matrix (ECM) found in cartilage and bone (Tao *et al*., 2020; Qi *et al*., 2021). HAp and chitosan nanocomposites (nHAp-CS) have been used in bone tissue engineering over the last decade. They have excellent osteoconductivity, biodegradability, biocompatibility, and osteogenesis (Ait Said *et al*., 2023).

The optimal biomaterial for bone regeneration should have one or a combination of the following characteristics: osteogenic, osteoinductive, and osteoconductive (Xie *et al*., 2021). Thus, the study's specific objectives were to assess the bone regenerative efficacy of a gelatin-based hemostatic sponge (Surgispon) in the treatment of segmental bone defects in the radius of rabbits as a standalone treatment or in combination with a 75/25 weight ratio hydroxyapatite–chitosan nanocomposites (nHAp/CS) composite.

Materials and Methods

Experimental animals

Eighteen male white New Zealand rabbits with an age range of 3 months, weighing 2.5 kg and ±0.5 kg, were selected and used. The rabbits were kept in separate cages with standard rabbit food pellets and water available *ad libitum*. They were housed in a room maintained at 25°C with a 12-hour light/dark cycle.

Materials

Surgispon was obtained from Aegis Lifesciences (Mahagujarat Industrial Estate, Ahmedabad, Gujarat, India). The nHAp/CS composite with a weight ratio of 75/25 was purchased from Nano Gate Company (Mokattam, Cairo Governorate, Egypt), which prepared and synthesized the nHAp/CS composite.

Experimental groups

The rabbits were subjected to 10-mm-induced full-thickness segmental defects at the mid-shaft of the radius of the left limb and randomly distributed into three groups according to the method of treatment. In group I, the defects were left untreated (control group) (n = 6). In group II, the defects were implanted with Surgispon (n = 6). In group III, the defects were implanted with a 75/25 weight ratio nHAp/CS composite wrapped with a Surgispon (n = 6).

For evaluation of the bone healing at the defect site in each group (n = 6), radiographic, gross, computed tomography (CT), and histopathological examinations were performed at 6 weeks (n = 3) and 12 weeks (n = 3) postoperatively.

Preoperative preparation and postoperative management

All animals were administered intramuscularly 20-mg/kg cefazolin sodium 1g (Zinol, Pharco Pharmaceuticals, Alexandria, Egypt) for 5 days (Demirel and Aksakal, 2015). The anti-inflammatory agent meloxicam 0.75% was given at 0.6 mg/kg subcutaneously (Amriya Pharmaceutical Industries, Alexandria, Egypt) for 24 hours over 3 days (Varga, 2014).

Anesthesia and control

The rabbits were premedicated with an intramuscular injection of acepromazine maleate 1.5% (Castran, Interchemie Co., The Netherlands) at a dose rate of 0.75 mg/kg, followed by a subcutaneous injection of xylazine 2% (Xyla, Interchemie Co., The Netherlands) at a dose rate of 5 mg/kg. The anesthesia was induced with an intramuscular injection of 5% ketamine hydrochloride (Panpharma Laboratory, Fougères, France) at a dose rate of 35 mg/kg (Boudra *et al*., 2020). The left forelimbs of all animals were prepared aseptically for surgical operation. After anesthesia was achieved, the rabbit was then placed on the operating table in the lateral position with the operated limb down most.

Surgical procedure

The surgical access of the radius and the performing-induced segmental bone defect were illustrated in Figure 1. Craniomedially, a 4-cm incision was made in the skin of the left forelimb, and the radius was exposed by dissecting the surrounding muscles. Subsequently, a 10-mm osteoperiosteal segmental defect was performed at a location 2 cm proximal to the carpus joint using an oscillating saw and irrigation. The incision was made with precision to prevent any damage to the ulna. In addition, the interosseous ligament was surgically cut, facilitating the removal of the fragment (Minto *et al*., 2020).

The defects were treated according to group allocation (Figure 1). Post-implantation, the radius did not require internal fixation because the ulna provided sufficient support, allowing for full weight bearing. Finally, the

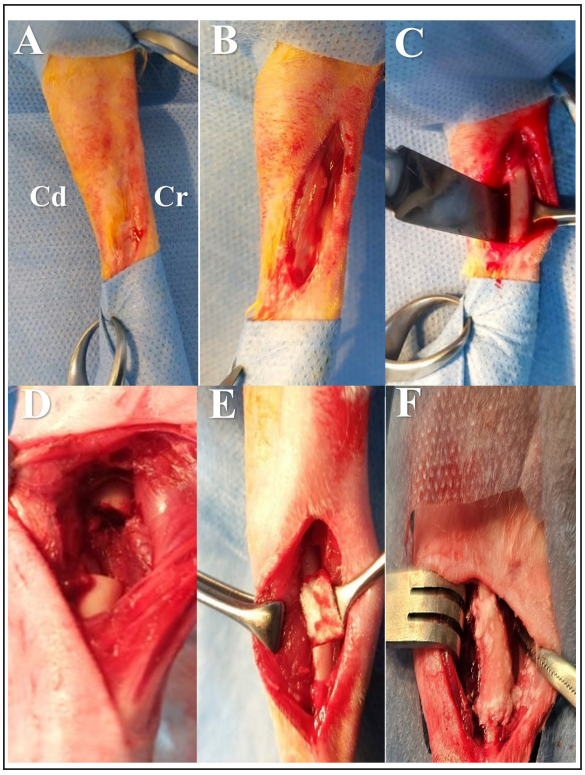

Fig. 1. Surgical procedure and the treatment groups. **(A)** Left radius prepared aseptically for surgical operation. **(Cd)** Caudal **(Cr)** Cranial. **(B)** 4-cm incision was made craniomedially in the skin of the left forelimb, and the radius bone was exposed by dissecting the surrounding muscles. **(C)** Exposed left radius. **(D)** Group I (the control group) was left empty. **(E)** Bone defect is filled with a Surgispon. **(F)** Bone defect is filled with a weight ratio 75/25 nHAp/CS composite wrapped with a Surgispon.

operative wound was closed routinely with 2/0 Vicryl (Egysorb, Obour City, Cairo, Egypt) for muscle and subcutaneous, and 3/0 braided silk sutures (EGYSILK, Taisier.Co-Med, Obour City, Egypt) for skin.

Following the surgical procedures, the rabbits were transferred to a recovery room, where they remained until they regained complete consciousness. The skin sutures were removed on the 7th postoperative day. During the experiment, the rabbits were fed *ad libitum*. All rabbits were sacrificed at 6 and 12 weeks after surgery for radiographic analysis, gross examination, CT scan, and histopathological examination.

Radiographic analysis

Immediately following surgery, using exposure factors (2.5 mAs, 40 kVp, and 50 mA), mediolateral radiographs of the radius using an X-ray machine (Pox-300 BT, Toshiba, Rotanode™, Japan) were taken. The radiographic examination was performed at 6 and 12 weeks postoperatively. The results were scored using the Lane–Sandhu system (Table 1) by two separate experts who were unaware of the different groups (Zhao *et al*., 2021).

Gross examination

After animals were sacrificed, the radius and ulna were harvested, and the soft tissue was removed at the 6th and 12th weeks postoperatively. The macroscopic observation of the bone defect was conducted and photographed. The harvested radius and ulna bones were examined and scored in a blinding manner using a scoring system, as previously described by (Parizi *et al*. (2013), considering the presence of bridging bone, which indicated a complete union, and were assigned a score of +3. In addition, the presence of cartilage, soft tissue, or cracks within the defect was assessed, indicating a potentially unstable union and assigning a score of +1 or +2. Finally, if there is complete instability at the defect site, indicating no union, a score of 0 was assigned.

CT scan

The harvested radius and ulnar bones of rabbits in each group were scanned at the 6th and 12th weeks using a GE Lightspeed VCT 64 CT device (WIPRO GE HEALTHCARE PVT. LTD., Karnataka, India). Images were reconstructed in coronal and three-dimensional (3D) and visualized using the RadiAnt DICOM viewer program (Medixant, Poznan, Poland). All radial bones were scanned with an energy value of 140 kV and 50 mA. The assessment of new bone formation at the defect site was conducted by two senior orthopedic specialists who were blinded using Cheung's scoring method (Table 2), as described previously by Ibrahim *et al*. (2016).

Histopathological examination

To perform histological evaluation, bone samples containing the defect were collected using a slow-speed saw. The bone samples were promptly placed in a 10% neutral buffered formalin solution for 48 hours. The samples preserved in formalin were then decalcified using mixtures of hydrochloric acid 10% and formic acid 10% for 3 weeks, dehydrated in gradually ascending ethanol, cleared in xylene, and embedded in paraffin wax. The paraffinized samples were cut in longitudinal serial slices using a microtome (Leica RM 2155, England), with a thickness of 5 µm from the central regions of each sample. These slices were then subjected to staining using hematoxylin and eosin (H and E) and Masson's trichrome. The sections were evaluated and scored by two pathologists using Emery's scoring system, with the evaluation process being blind (Table 3) (Emery *et al*., 1994).

Statistical analysis

The data provided was presented in the form of means and standard deviations. The statistical software GraphPad Prism version 10.3.0 (GraphPad Software, La Jolla, CA, USA) was utilized for data analysis. Differences are regarded as significant when the *p*-values are less than 0.05. They are considered highly

Table 1. Lane–Sandhu radiographic scoring system.

Category	Standard	Scores
Bone formation	No evidence of bone formation	0
	Bone formation occupying 25% of defect	1
	Bone formation occupying 50% of defect	2
	Bone formation occupying 75% of defect	3
	Full gap bone formation	4
Fracture line	Clear	0
	Relatively clear	1
	Partial fracture line	2
	Basically vanished	3
	Completely vanished	4
Bone remodeling	No evidence of remodeling	0
	Remodeling of medullary canal	2
	Full remodeling of cortex	4

Table 2. Cheung's scoring method.

Grade	Radiographic description
Grade 1	Indicates no calcification at the fracture site.
Grade 2	Indicates patchy calcification
Grade 3	Indicates that the calcification takes on the appearance of the callus
Grade 4	Shows callus bridging across the fracture gap
Grade 5	Indicates continuity of bone trabeculae
Grade 6	Demonstrates remodeling to normal bone

significant when the *p*-values are less than 0.01 and less than 0.001.

Ethical approval

The experimental protocol was approved by the Zagazig University Committee of Animal Welfare and Research Ethics.

Results

Radiographic findings

The mediolateral radiograph was obtained immediately following the surgical procedure. The radiographs in group I were radiolucent, while those in group II were marginally radiopaque. Group III radiographs serve as illustrations of radiopaque density (Fig. 2).

Following 6 weeks post-implantation, the radiographs of the segmental bone defect in group I showed a lack of bone union and considerably reduced radiopacity when compared to the neighboring healthy bone, indicating that bone regeneration is limited. Compared to group I, groups II and III showed a significant reduction in the extent of defects due to enhanced bone regeneration but without identifying the bone union (Fig. 2).

Table 3. Histological examination Emery's scoring system.

Item	Score
Empty gap	0
Filled with fibrous connective tissue only	1
More fibrous tissue than fibrocartilage	2
More fibrocartilage than fibrous tissue	3
Fibrocartilage only	4
More fibrocartilage than bone	5
More bone than fibrocartilage	6
Filled only with bone	7

At 12 weeks (Fig. 2), radiographic findings suggested that there was no apparent bone union in group I. Group II evidenced improved bone growth in contrast to group I, which successfully achieved bone union. In addition, the repaired segment was thinner than the healthy bone that was close to it. The remarkable enhancement in bone formation observed in group III had the effect of achieving complete bone union.

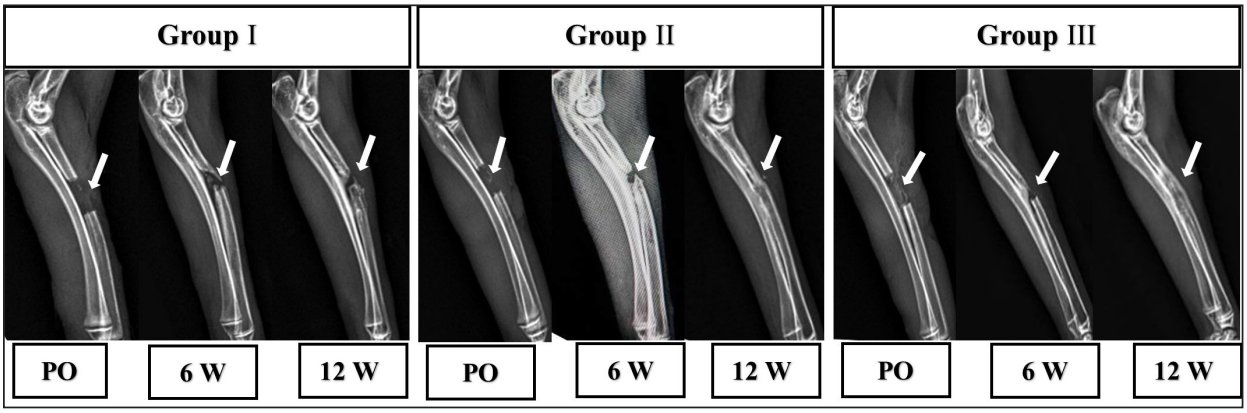

Fig. 2. The mediolateral radiographs of groups I–III were obtained immediately following the surgical procedure (PO) and at 6- and 12-week post-surgical intervention. The white arrow clearly shows the defect's location and the progress of healing.

According to the findings of radiographic statistical analysis (Fig. 3A), there were no significant differences between the groups at 6 weeks in terms of defect healing, as evaluated using the Lane–Sandhu radiographic score ($p > 0.05$). However, at 12 weeks, there were highly significant differences observed between groups I and II ($p = 0.006$), as well as between groups I and III ($p = 0.002$). However, there were no notable statistical differences observed between groups II and III.

Gross findings

In gross examinations at 6 weeks (Fig. 4), the gap in group I remained unclosed and was filled with fibrous tissue, while the gap was also visible in group II, but it was smaller in diameter. Group III exhibited bone segment stability and partial repair.

The defect in group I at 12 weeks was clearly visible, with fibrous-like tissue filling the space between the defects. However, in groups II and III, complete bone healing was observed 12 weeks post-surgical operation (Fig. 4).

In the gross examination statistical analysis, there were no statistically significant differences in these scores between the groups at six weeks (Figure 3.B). At 12 weeks, the quantification data of the gross examination revealed that the regenerated area of the radius defect was statistically significant in groups III and II in comparison to group I, $p = 0.041$ (Fig. 3B).

CT findings

The 3D CT images of the 6-week postoperative groups, as illustrated in (Fig. 5), showed that in group I, the bone defect was clear with a well-defined appearance. Group II had a persistent and distinct fracture line, indicating a lack of bone trabeculae connection, but the defect was smaller in size than group I, so distinct new bone formation. In group III, the CT 3D revealed bone trabeculae continuity, but new bone growth was confined to the uni-cortical bone next to the ulnar bone. The edges of the bone defects in group I were clearly defined, and a reduction in the diameter of the defects was observed 12 weeks postoperatively, as illustrated in Fig. 5. The bone defect in groups II and III at 12 weeks was completely filled with bone and vanished (Fig. 5). The bone trabeculae continuity was well defined.

The quantitative results of CT, which were obtained using Cheung's scoring method, indicated that there were no statistically significant differences between the groups at 6 weeks following surgery ($p > 0.05$). Group III had the highest score at 12 weeks post-surgery, and statistically significant differences were evident between groups I and III ($p = 0.0065$) and groups I and II ($p = 0.029$). However, there were no statistically significant differences between groups II and III (Figure 3C).

Histopathological findings

In group I at 6 weeks stained with H and E (Fig. 6A), the defect site was filled with more fibrous connective tissue and an organized fibrocartilaginous mass. The same group stained with Masson's trichrome showed more fibrocartilaginous areas with prominent collagen bundles between abundant fibrous connective tissue (Fig. 7A). Group II at 6 weeks, stained with H and E (Fig. 6C), revealed calcified cartilage, immature osseous tissue around "inserted material," and highly cellular immature fibrous tissue with osteoclast cells filling the gap. Fibrocartilage surrounds chondroblastic and osteoblastic metaplasia. Staining with Masson's trichrome exhibited a large area of fibrocartilage with abundant collagen contents that adhered to fibrous tissue. Chondroblastic and osteoblastic metaplasia were also noticed (Fig. 7C). The H and E staining section in group III at 6 weeks revealed immature bone tissue with osteoblast cells surrounded by fibrous connective tissue, hyaline cartilage, and calcified cartilaginous tissue (Fig. 6E). Masson's trichrome stained a large area of fibrocartilage, more fibrovascular tissue, and less immature bone tissue (Fig. 7E).

Group I at 12 weeks, sectioning stained with H and E, was filled with trabecular bone tissue, calcified cartilage, and fibrotic marrow spaces. The osteoblastic activity was also seen between mature

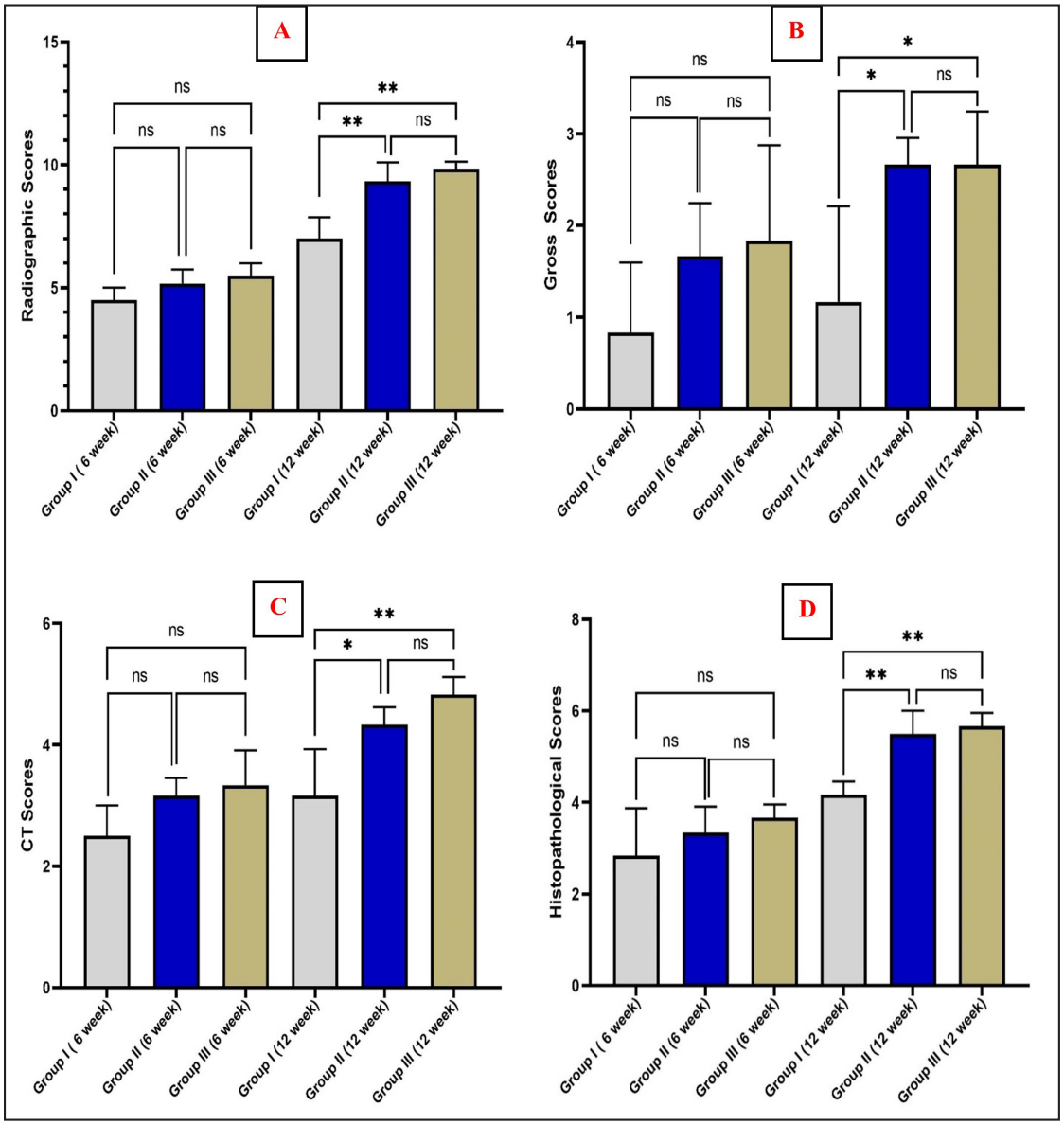

Fig. 3. Graphs quantitatively represent **(A)** Lane–Sandhu Radiographic Scoring System, **(B)** gross examination scoring system, **(C)** CT using Cheung's scoring method, and **(D)** histological examinations using Emery's scoring system. The "ns" denoted the absence of a statistically significant difference. The asterisk (*) indicated that there was a statistically significant difference with a *p*-value of less than 0.05, while (**) indicated that there was a highly statistically significant difference with a *p*-value of less than 0.01.

chondrocytes and newly formed bone (Fig. 6B). Masson's trichrome presented mature cartilaginous and fibrous tissue adhering to mature and immature bone tissue. Impacted osteoblastic and osteoclastic activity in marrow spaces was seen (Fig. 7B). The histopathological examination of group II, which employed the H and E stain, proved the presence of calcified cartilaginous material, osseous tissue, and a core of less cellular fibrous tissue. Bone marrow spaces that contained osteoblast cells were also observed (Fig. 6D). In Group II, Masson's trichrome, immature cartilaginous and bony tissue was seen alongside small areas of mature bone and fibrous connective tissue. Marrow contained osteoclasts, osteoblasts, and active fibrous tissue (Fig. 7D). Group III at 12 weeks had mature, well-organized lamellar osseous tissue around the Haversian canals and a few calcified cartilaginous tissues at the defect site (Fig. 6F). The same group Masson's trichrome identified mature lamellar bony tissue as "pink color," an extensive area

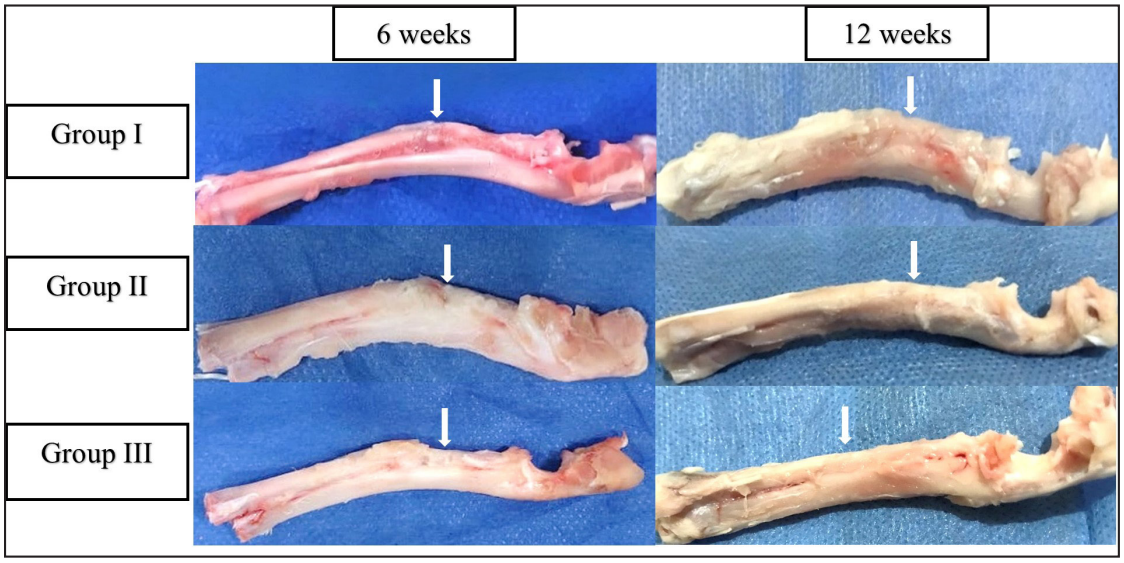

Fig. 4. Gross examinations were performed in groups I–III at 6 and 12 weeks postoperatively, with white arrows indicating defect locations.

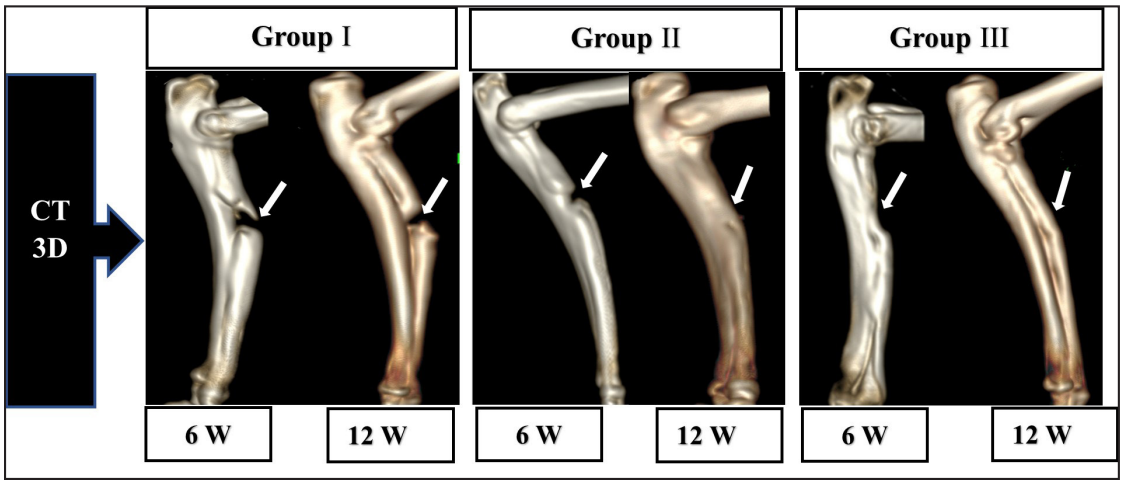

Fig. 5. Three-dimensional CT (CT) images were obtained for groups I–III at 6 and 12 weeks postoperatively. The stage of healing was indicated by the white arrow mark on the 10-mm-induced full-thickness segmental defect at the mid-shaft of the radius in each image.

of immature bone and hyaline cartilage, and a fibrous tissue core. Also, active osteoblasts filled marrow spaces (Fig. 7F).

Figure 3D displays the statistical findings from the use of Emery's scoring system for histopathological examinations. These results did not reveal any noticeable statistically significant variation between the groups 6 weeks postoperatively. The quantitative histopathological results for groups II and III at 12 weeks post-surgical operation, as shown in (Figure 3D), proved that both groups were superior to group I. In addition, a statistically significant difference was observed, with a *p*-value of less than 0.01.

Discussion

Gelatin is commonly employed in the field of biomedicine. In its denatured state, gelatin is reserved of tripeptide sequences called RGD (arginyl–glycine–aspartic acid). These sequences play a role in facilitating cellular interactions with the ECM. This biomimetic peptide demonstrates improved cellular adhesion, differentiation, and proliferation (Kurian *et al*., 2022). The hemostatic gelatin sponge has shown considerable promise as a scaffold for bone tissue engineering, as evidenced by various studies conducted in vivo and in vitro. These investigations provide in vitro outcomes, which include good biodegradability and

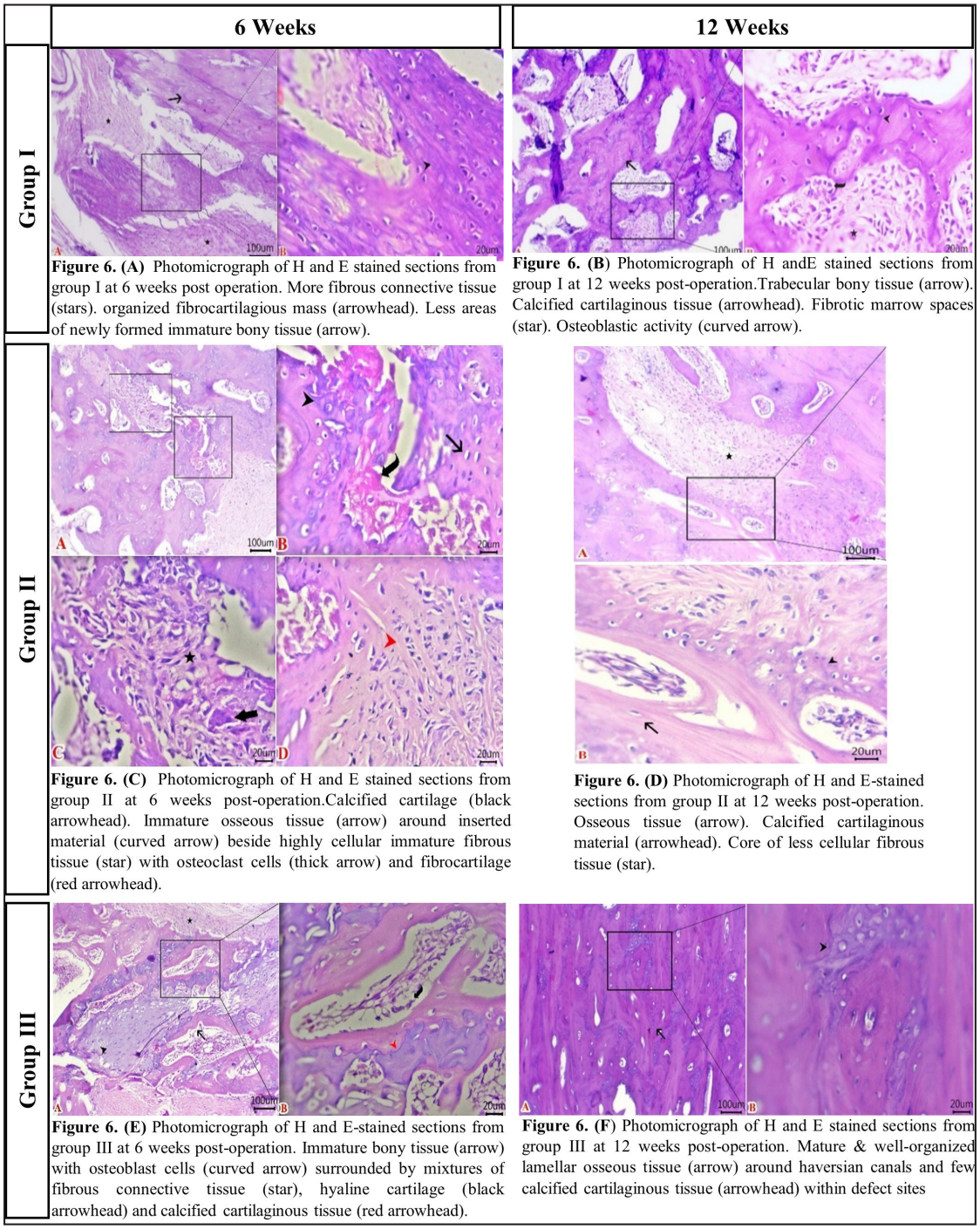

Figure 6. (A) Photomicrograph of H and E stained sections from group I at 6 weeks post operation. More fibrous connective tissue (stars). organized fibrocartilagious mass (arrowhead). Less areas of newly formed immature bony tissue (arrow).

Figure 6. (B) Photomicrograph of H andE stained sections from group I at 12 weeks post-operation.Trabecular bony tissue (arrow). Calcified cartilaginous tissue (arrowhead). Fibrotic marrow spaces (star). Osteoblastic activity (curved arrow).

Figure 6. (C) Photomicrograph of H and E stained sections from group II at 6 weeks post-operation.Calcified cartilage (black arrowhead). Immature osseous tissue (arrow) around inserted material (curved arrow) beside highly cellular immature fibrous tissue (star) with osteoclast cells (thick arrow) and fibrocartilage (red arrowhead).

Figure 6. (D) Photomicrograph of H and E-stained sections from group II at 12 weeks post-operation. Osseous tissue (arrow). Calcified cartilaginous material (arrowhead). Core of less cellular fibrous tissue (star).

Figure 6. (E) Photomicrograph of H and E-stained sections from group III at 6 weeks post-operation. Immature bony tissue (arrow) with osteoblast cells (curved arrow) surrounded by mixtures of fibrous connective tissue (star), hyaline cartilage (black arrowhead) and calcified cartilaginous tissue (red arrowhead).

Figure 6. (F) Photomicrograph of H and E stained sections from group III at 12 weeks post-operation. Mature & well-organized lamellar osseous tissue (arrow) around haversian canals and few calcified cartilaginous tissue (arrowhead) within defect sites

Fig. 6. Histological examination sections stained with H and E (scale bar 100 µm and high magnification at 20 µm). (A) Group I at 6 weeks. (B) Group I at 12 weeks. (C) Group II at 6 weeks. (D) Group II at 12 weeks. (E) Group III at 6 weeks. (F) Group III at 12 weeks.

biocompatibility, osteogenic differentiation, and the migration of preosteoblasts, while in vivo data suggest properly directed bone regeneration (Rohanizadeh *et al*., 2008; Sohn *et al*., 2010; Kuo *et al*., 2016; Ashour *et al*., 2018; Wang *et al*., 2019; Wähnert *et al*., 2021).

Bio-nanocomposites, such as nHAp/CS, are designed to enhance not only their mechanical properties but also their biodegradability, osteoconductivity, and bioactivity when compared to the individual components (Thein-Han and Misra, 2009; Sun *et al*., 2014). The nHAp/CS

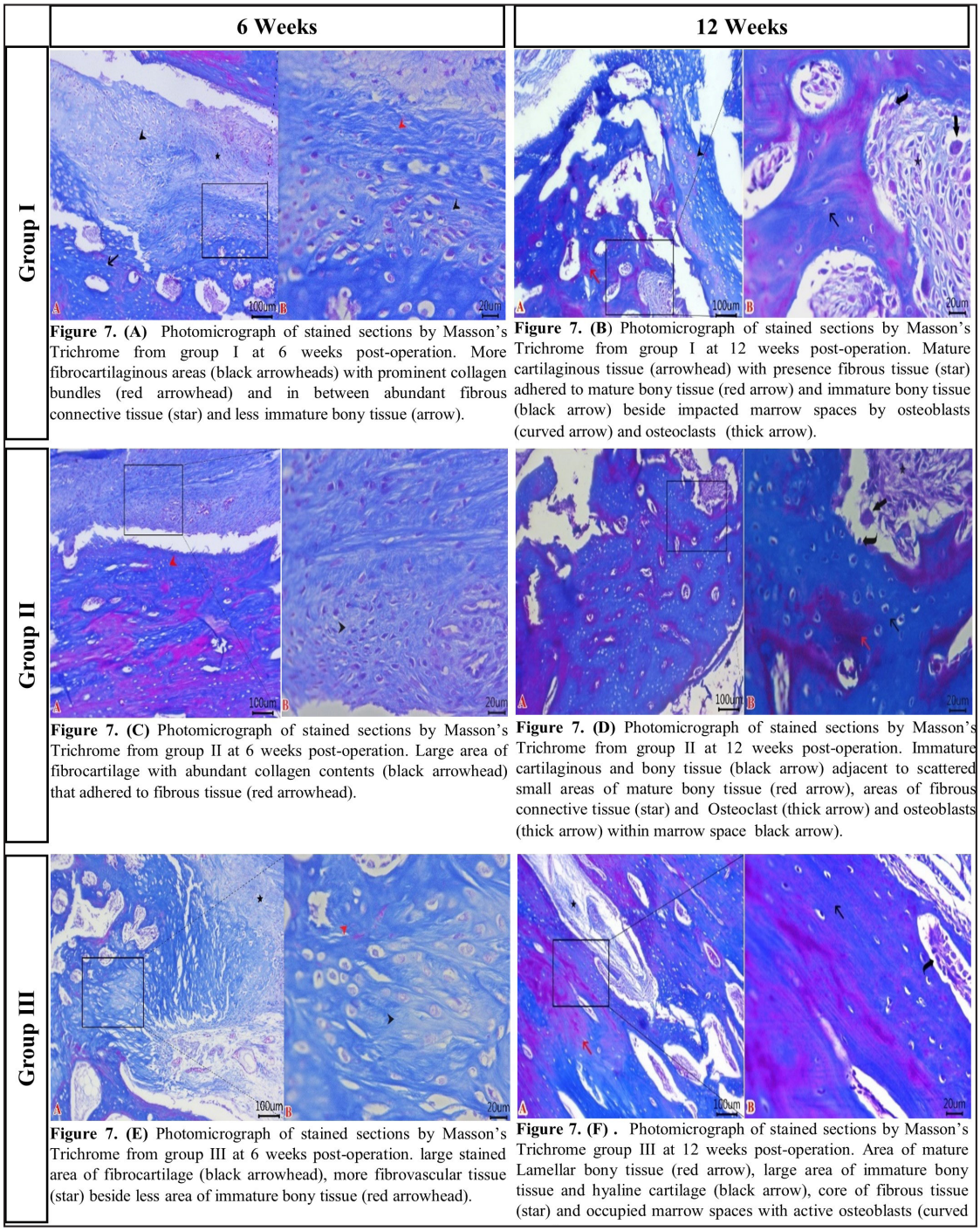

Figure 7. (A) Photomicrograph of stained sections by Masson's Trichrome from group I at 6 weeks post-operation. More fibrocartilaginous areas (black arrowheads) with prominent collagen bundles (red arrowhead) and in between abundant fibrous connective tissue (star) and less immature bony tissue (arrow).

Figure 7. (B) Photomicrograph of stained sections by Masson's Trichrome from group I at 12 weeks post-operation. Mature cartilaginous tissue (arrowhead) with presence fibrous tissue (star) adhered to mature bony tissue (red arrow) and immature bony tissue (black arrow) beside impacted marrow spaces by osteoblasts (curved arrow) and osteoclasts (thick arrow).

Figure 7. (C) Photomicrograph of stained sections by Masson's Trichrome from group II at 6 weeks post-operation. Large area of fibrocartilage with abundant collagen contents (black arrowhead) that adhered to fibrous tissue (red arrowhead).

Figure 7. (D) Photomicrograph of stained sections by Masson's Trichrome from group II at 12 weeks post-operation. Immature cartilaginous and bony tissue (black arrow) adjacent to scattered small areas of mature bony tissue (red arrow), areas of fibrous connective tissue (star) and Osteoclast (thick arrow) and osteoblasts (thick arrow) within marrow space black arrow).

Figure 7. (E) Photomicrograph of stained sections by Masson's Trichrome from group III at 6 weeks post-operation. large stained area of fibrocartilage (black arrowhead), more fibrovascular tissue (star) beside less area of immature bony tissue (red arrowhead).

Figure 7. (F) . Photomicrograph of stained sections by Masson's Trichrome group III at 12 weeks post-operation. Area of mature Lamellar bony tissue (red arrow), large area of immature bony tissue and hyaline cartilage (black arrow), core of fibrous tissue (star) and occupied marrow spaces with active osteoblasts (curved

Fig. 7. Histological examination sections stained with Masson's trichrome (scale bar 100 µm and high magnification at 20 µm). **(A)** Group I at 6 weeks. **(B)** Group I at 12 weeks. **(C)** Group II at 6 weeks. **(D)** Group II at 12 weeks. **(E)** Group III at 6 weeks. **(F)** Group III at 12 weeks.

composite has been proven to stimulate the growth of new bone in experimental animal models. Injectable nHAP/CS composite scaffolds and pure CS scaffolds were both implanted into rabbits with femoral condyles that made defects of essential dimensions (6 mm in diameter and 10 mm in length) to evaluate their potential for bone regeneration. Twelve weeks following surgery, the segmental bone defect in the nHAp/CS group had completely healed, but in the CS group, the defect was still apparent (Zhang *et al*., 2012).

The present study assessed the ability of Surgispon and its combination with a nHAp/CS weight ratio of 75/25 to promote bone regeneration in rabbits with 10-mm segmental radius defects. The method of evaluation involved the use of X-rays and CT scans, along with detailed macroscopic and microscopic images of histopathological sections taken at 6 and 12 weeks postoperatively. The statistical analysis revealed that there was no notable difference between the groups at 6 weeks post-surgical intervention. The results of the 12-week postoperative time showed that groups II and III were significantly different from group I in all quantitative measurements of different evaluation methods.

Two recent studies investigated the in vivo efficacy of a gelatin-based hemostatic sponge (Spongostan). The study treated rats with critical-sized calvarial defects with Spongostan alone, collagen fibers, and Spongostan coated with silicon dioxide nanoparticles. The results showed that utilizing only Spongostan was the most positive in terms of a considerable increase in bone volume and complete defect healing at 4 weeks (Vordemvenne *et al*., 2020). Another study repaired a 5-mm biparietal defect in male white Wistar rats using Spongostan, NanoBone® (calcium phosphate bone substitute with silicate substitution), and Actifuse (nanocrystalline HAp and nanostructured silica gel). Spongostan promoted bone healing more effectively than the other two materials at 4 weeks post-surgical operation (Wähnert *et al*., 2021). The present study was consistent with the results of two experimental studies in which a hemostatic gelatin sponge is capable of bone formation. However, our analysis showed that the bone generation was greater when the Surgispon was incorporated with a weight ratio of 75/25 nHAp/CS composite. It seems that NanoBone and Actifuse are biomaterials with only osteoconductive properties (Harms *et al*., 2012; Harshavardhana and Noordeen, 2015).

Nanocomposites (nHAp/CS) used in current experiments have been shown to be effective biomaterials for bone regeneration in a variety of studies due to their multiple desired features. It has the ability to provide a framework for bone growth and development. In addition, nHAp/CS possesses the inherent capacity of biomaterials to induce the formation of bone tissue and directly provide for and support the growth of osteoblasts and osteoprogenitor cells, thereby facilitating the process of bone formation. Interestingly, previous studies have provided evidence supporting the use of inorganic–organic nanocomposites, particularly nHAp-CS with a weight ratio of 75/25 and 70/30, as biomaterials that effectively promote bone regeneration. Experimental investigation in vivo was carried out to examine the osteogenic potential of the nHAp/CS scaffold with a weight ratio of 75/25 upon implantation in an adult Sprague-Dawley rat model with a critical-sized calvarial bone defect. Based on the histological and histomorphometric observations, the researchers conclude that scaffolds composed of nHAp/CS with a weight ratio of 75/25 are effective for new bone formation (Chatzipetros *et al*., 2021). Also, the clinical study was conducted to evaluate the efficacy of a 70/30 weight ratio nHAp-CS composite in the regenerative and repair of bony defects in the maxilla or mandible that were caused by cysts or tumors. The results indicate a substantial reduction in the extent of bone defects and an increase in bone density in those treated with nHAp-CS composite (Abd *et al*., 2021). In the present experimental study, Surgispon was employed as a scaffold for nHAp/CS in powder form. Consequently, it was not feasible to incorporate an additional group as the sole biomaterial for nHAp/CS due to the materials' powder form, which made it challenging to implant them in the radius bone. However, the results of the current study definitively indicate that the incorporation of nHAp/CS composites at a weight ratio of 75/25 into Surgispon significantly improved bone regeneration in the treatment segmental defect that was induced in the mid diaphyseal radius of rabbits. The considerable increase in bone regeneration was attributed to the addition of the nHAp/CS composites, as the Surgispon alone was less effective in promoting bone formation than the combination.

The study findings indicated important statistically significant differences in quantitative assessment of bone repair between groups II and III compared to group I, 12 weeks postoperatively. As a result, the healing time in the present study was 12 weeks post-implantation. In the experiments mentioned by Wähnert *et al*. (2021) and Vordemvenne *et al*. (2020), a hemostatic gelatin sponge was used to aid 5-mm critical-sized calvarial defects in rats. The results showed that complete bony closure was achieved at 4 weeks. The study by Hatakeyama *et al*. (2023) involved analyzing the effects of implanting spongy gelatin disks into rat calvaria defects. There was an identifiable increase in bone volume observed 8 weeks after the post-implantation. To the best of the authors' knowledge, there is no published research data incorporating the nHAp/CS composite with hemostatic gelatin sponge to investigate the healing potential for repairing the bony defects. The healing time of our investigation is distinct from that of the previously discussed studies. The healing period for mice and rats is shorter compared to other animals after a fracture due to their unique repair process that involves intramembranous ossification (Gao *et al*., 2023). This discrepancy may possibly arise from the fact that the process of bone healing in the calvaria, which is a nonload-bearing anatomical site, differs from that in long bones, which are load bearing. The formation of the majority of bones occurs through endochondral ossification, where mesenchymal cells derived from mesoderms play a crucial role. The cells undergo a process of differentiation into intermediate chondrocytes before ultimately transforming into bone.

However, the calvarial bone is formed by the neural crest and mesoderm, which play an integral part in its development through a direct process of transmutation into bone called intramembranous ossification. Quarto *et al*. (2010) have determined that tissue originating from the neural crest has a greater capacity for bone formation and repair compared to tissue generated from the mesoderm. Some authors pointed out that neural crest-derived cells have been found to produce a greater amount of mineralized tissue and stimulate more bone formation compared to mesoderm-derived cells from long bones (Aghaloo *et al*., 2010; Reichert *et al*., 2013).

Conclusion

The results of this study reinforce the potential of Surgispon to promote bone regeneration. In addition, Surgispon functioned effectively as scaffolds for the nHAp/CS composite at a weight ratio of 75/25. The incorporation of nHAp/CS composite into Surgispon significantly improved their ability to enhance bone regeneration in the treatment of 10-mm segmental defects in the rabbit's radii. The combination of both Surgispon and nHAp/CS composite could offer valuable insights for the treatment of bone defects and, in the long term, enhance bone regeneration.

Acknowledgments

The authors extend their gratitude to the staff members of the Surgery Department, Faculty of Veterinary Medicine, Zagazig University, Egypt, for their steadfast assistance and support.

Funding

None.

Authors' contributions

The experimental design was developed by F.D.E., M.G., S.A.E., M.A., and T.N.E. T.N.E., and M.A. surgical intervention. F.D.E., M.G., and S.A.E. surgical supervision. T.N.E. Postoperative management. T.N.E., and M.A data collection and management. T.N.E. analyzed and interpreted the data and wrote the original draft of the manuscript. F.D.E. Supervision. All authors reviewed and approved the final manuscript.

Data availability

The manuscript contains all data pertaining to the study's findings.

References

Abd EL Hafez, D.M., Ali, T.M. and El Ashwah, A.A. 2021. Evaluation of chitosan/hydroxyapatite scaffold on the healing of osseous defects in jaw bones (clinical study). Alex. Dent. J. 46(1), 6–14.

Aghaloo, T.L., Chaichanasakul, T., Bezouglaia, O., Kang, B., Franco, R., Dry, S.M., Atti, E. and Tetradis, S. 2010. "Osteogenic potential of mandibular vs. long-bone marrow stromal cells." J. Dent. Res. 89(11), 1293–1298.

Ait Said, H., Mabroum, H., Lahcini, M., Oudadesse, H., Barroug, A., Ben Youcef, H. and Noukrati, H. 2023. Manufacturing methods, properties, and potential applications in bone tissue regeneration of hydroxyapatite-chitosan biocomposites: a review. Int. J. Biol. Macromol. 243, 125150.

Ashour, A., Zaghloul, M., Mahmoud, W., Helal, M. and Grawish, M. 2018. Gelfoam haemostatic agent with or without autologous bone marrow-derived stem cells for the regeneration of critical-size mandibular defects in the rabbit. Int. J. Oral Maxillofac. Surg. 47(11), 1488–1494.

Boudra, A., Benbelkacem, I., Merati, R., Achour, H. and Daouadji, I.D. 2020. Comparison between three fixed anaesthesia protocols in rabbits. J. Prev. Vet. Med. 44(3), 99–103.

Chatzipetros, E., Damaskos, S., Tosios, K.I., Christopoulos, P., Donta, C., Kalogirou, E.M., Yfanti, Z., Tsiourvas, D., Papavasiliou, A. and Tsiklakis, K. 2021. The effect of nano-hydroxyapatite/chitosan scaffolds on rat calvarial defects for bone regeneration. Int. J. Implant Dent. 7(1), 1–11.

Demirel, M. and Aksakal, B. 2015. Enhanced bone regeneration in rabbit tibial defects implanted with newly fabricated bioceramic bone grafts. Int. J. Appl. Ceram. 12(2), 254–263.

Dimitriou, R., Jones, E., McGonagle, D. and Giannoudis, P.V. 2011. Bone regeneration: current concepts and future directions. BMC Med. 9(1), 66.

Emery, S.E., Brazinski, M.S., Koka, A., Bensusan, J.S. and Stevenson, S. 1994. The biological and biomechanical effects of irradiation on anterior spinal bone grafts in a canine model. JBJS 76(4), 540–548.

Gao, H., Huang, J., Wei, Q. and He, C. 2023. Advances in animal models for studying bone fracture healing. Bioeng. 10(2), 201.

Georgeanu, V.A., Gingu, O., Antoniac, I.V. and Manolea, H.O. 2023. Current options and future perspectives on bone graft and biomaterials substitutes for bone repair, from clinical needs to advanced biomaterials research. Appl. Sci. 13(14), 8471.

Harms, C., Helms, K., Taschner, T., Stratos, I., Ignatius, A., Gerber, T., Lenz, S., Rammelt, S., Vollmar, B. and Mittlmeier, T. 2012. Osteogenic capacity of nanocrystalline bone cement in a weight-bearing defect at the ovine tibial metaphysis. Int. J. Nanomedicine 7, 2883–2889.

Harshavardhana, N.S. and Noordeen, M.H. 2015. Surgical results with the use of silicated calcium phosphate (SiCaP) as bone graft substitute in posterior spinal fusion (psf) for adolescent idiopathic scoliosis (AIS). Scoliosis 10, 27.

Hatakeyama, T., Hamai, R., Shiwaku, Y., Anada, T., Sakai, S., Sato, T., Baba, K., Sasaki, K. and Suzuki, O. 2023. Effects of degradation products

from gelatin spongy scaffolds on angio-osteogenic capacity. Sci. Technol. Adv. Mater. 24(1), 2277675.

Ibrahim, M.R.M., Singh, S., Merican, A.M., Raghavendran, H.R.B., Murali, M.R., Naveen, S.V. and Kamarul, T. 2016. The effect of strontium ranelate on the healing of a fractured ulna with bone gap in rabbit. BMC Vet. Res. 12(1), 1–9.

Jo, Y.Y., Kim, S.G., Kwon, K.J., Kweon, H., Chae, W.S., Yang, W.G., Lee, E.Y. and Seok, H. 2017. Silk fibroin-alginate-hydroxyapatite composite particles in bone tissue engineering applications in vivo. Int. J. Mol. Sci. 18(4), 858.

Jyoti, J., Kiran, A., Sandhu, M., Kumar, A., Singh, B.P. and Kumar, N. 2021. Improved nanomechanical and in-vitro biocompatibility of graphene oxide-carbon nanotube hydroxyapatite hybrid composites by synergistic effect. J. Mech. Behav. Biomed. Mater. 117, 104376.

Kuo, Z.K., Lai, P.L., Toh, E.K.W., Weng, C.H., Tseng, H.W., Chang, P.Z., Chen, C.C. and Cheng, C.M. 2016. Osteogenic differentiation of preosteoblasts on a hemostatic gelatin sponge. Sci. Rep. 6(1), 32884.

Kurian, A.G., Singh, R.K., Patel, K.D., Lee, J.H. and Kim, H.W. 2022. Multifunctional GelMA platforms with nanomaterials for advanced tissue therapeutics. Bioact. Mater. 8, 267–295.

Kuttappan, S., Mathew, D. and Nair, M.B. 2016. Biomimetic composite scaffolds containing bioceramics and collagen/gelatin for bone tissue engineering-a mini review. Int. J. Biol. Macromol. 93, 1390–1401.

Laubach, M., Hildebrand, F., Suresh, S., Wagels, M., Kobbe, P., Gilbert, F., Kneser, U., Holzapfel, B.M. and Hutmacher, D.W. 2023. The concept of scaffold-guided bone regeneration for the treatment of long bone defects: current clinical application and future perspective. J. Funct. Biomater. 14(7), 341.

Lei, X., Gao, J., Xing, F., Zhang, Y., Ma, Y. and Zhang, G. 2019. Comparative evaluation of the physicochemical properties of nano-hydroxyapatite/collagen and natural bone ceramic/collagen scaffolds and their osteogenesis-promoting effect on MC3T3-E1 cells. Regen. Biomater. 6(6), 361–371.

Li, C., Qin, W., Lakshmanan, S., Ma, X., Sun, X. and Xu, B. 2020. Hydroxyapatite based biocomposite scaffold: a highly biocompatible material for bone regeneration. Saudi J. Biol. Sci. 27(8), 2143–2148.

Minto, B., Neto, J.G., Sprada, A., Quarterone, C., Sartori, M., de Alcântara, B., Hespanha, A. and Uscategui, R. 2020. A critical size defect model in the radius of rabbits. Ars Vet. 36(3), 187–194.

Miron, R.J. 2024. Optimized bone grafting. Periodontol. 2000 94(1), 143–160.

Paganelli, C., Fontana, P., Porta, F., Majorana, A., Pazzaglia, U. and Sapelli, P. 2006. Indications on suitable scaffold as carrier of stem cells in the alveoloplasty of cleft palate. J. Oral Rehabil. 33(8), 625–629.

Parizi, A.M., Oryan, A., Shafiei-Sarvestani, Z. and Bigham-Sadegh, A. 2013. Effectiveness of synthetic hydroxyapatite versus Persian Gulf coral in an animal model of long bone defect reconstruction. J. Orthop. Traumatol. 14(4), 259–268.

Qi, J., Yu, T., Hu, B., Wu, H. and Ouyang, H. 2021. Current biomaterial-based bone tissue engineering and translational medicine. Int. J. Mol. Sci. 22(19), 10233.

Quarto, N., Wan, D.C., Kwan, M.D., Panetta, N.J., Li, S. and Longaker, M.T. 2010. Origin matters: differences in embryonic tissue origin and wnt signaling determine the osteogenic potential and healing capacity of frontal and parietal calvarial bones. J. Bone Miner. Res. 25(7), 1680–1694.

Reichert, J.C., Gohlke, J., Friis, T.E., Quent, V.M.C. and Hutmacher, D.W. 2013. Mesodermal and neural crest derived ovine tibial and mandibular osteoblasts display distinct molecular differences. Gene 525(1), 99–106.

Rohanizadeh, R., Swain, M.V. and Mason, R.S. 2008. Gelatin sponges (Gelfoam®) as a scaffold for osteoblasts. J. Mater. Sci. Mater. Med. 19, 1173–1182.

Sagar, V., Patel, D., Patel, P., Kumar, A., Rana, A. and Trivedi, B. 2022. Clinical studies on performance and safety of absorbable gelatin sponge - real world clinical experience (RWCE) with Surgispon®. Br. J. Bio. Med. Res. 6(2), 2022–2029.

Salamanca, E., Choy, C.S., Aung, L.M., Tsao, T.C., Wang, P.H., Lin, W.A., Wu, Y.F. and Chang, W.J. 2023. 3D-printed PLA scaffold with fibronectin enhances in vitro osteogenesis. Polym. 15(12), 2619.

Sohn, D.S., Moon, J.W., Moon, K.N., Cho, S.C. and Kang, P.S. 2010. New bone formation in the maxillary sinus using only absorbable gelatin sponge. J. Oral Maxillofac. Surg. 68(6), 1327–1333.

Sun, T., Khan, T.H. and Sultana, N. 2014. Fabrication and in vitro evaluation of nanosized hydroxyapatite/chitosan-based tissue engineering scaffolds. J. Nanomater. 2014, 11.

Tao, F., Cheng, Y., Shi, X., Zheng, H., Du, Y., Xiang, W. and Deng, H. 2020. Applications of chitin and chitosan nanofibers in bone regenerative engineering. Carbohydr. Polym. 230, 115658.

Thein-Han, W.W. and Misra, R.D. 2009. Biomimetic chitosan-nanohydroxyapatite composite scaffolds for bone tissue engineering. Acta Biomater. 5(4), 1182–1197.

Varga, M. 2014. Therapeutics. textbook of rabbit medicine (second edition). Oxford, UK: Butterworth-Heinemann, pp: 137–177.

Vordemvenne, T., Wähnert, D., Koettnitz, J., Merten, M., Fokin, N., Becker, A., Büker, B., Vogel, A.,

Kronenberg, D., Stange, R., Wittenberg, G., Greiner, J.F., Hütten, A., Kaltschmidt, C. and Kaltschmidt, B. 2020. Bone regeneration: a novel osteoinductive function of spongostan by the interplay between its nano- and microtopography. Cell J. 9(3), 654.

Wähnert, D., Koettnitz, J., Merten, M., Kronenberg, D., Stange, R., Greiner, J.F., Kaltschmidt, C., Vordemvenne, T. and Kaltschmidt, B. 2021. Spongostan™ leads to increased regeneration of a rat calvarial critical size defect compared to NanoBone® and actifuse. J. Mater. 14(8), 1961.

Wang, C.Y., Kuo, Z.K., Hsieh, M.K., Ke, L.Y., Chen, C.C., Cheng, C.M. and Lai, P.L. 2019. Cell migration of preosteoblast cells on a clinical gelatin sponge for 3D bone tissue engineering. Biomed. Mater. 15(1), 015005.

Wang, W. and Yeung, K.W.K. 2017. Bone grafts and biomaterials substitutes for bone defect repair: a review. Bioact. Mater. 2(4), 224–247.

Xie, C., Ye, J., Liang, R., Yao, X., Wu, X., Koh, Y., Wei, W., Zhang, X. and Ouyang, H. 2021. Advanced strategies of biomimetic tissue-engineered grafts for bone regeneration. Adv. Healthc. Mater. 10(14), 2100408.

Yu, W., Jiang, G., Liu, D., Li, L., Tong, Z., Yao, J. and Kong, X. 2017. Transdermal delivery of insulin with bioceramic composite microneedles fabricated by gelatin and hydroxyapatite. Mater. Sci. Eng. C 73, 425–428.

Zhang, X., Zhu, L., Lv, H., Cao, Y., Liu, Y., Xu, Y., Ye, W. and Wang, J. 2012. Repair of rabbit femoral condyle bone defects with injectable nanohydroxyapatite/chitosan composites. J. Mater. Sci. Mater. Med. 23, 1941–1949.

Zhao, L., Zhao, J., Tuo, Z. and Ren, G. 2021. Repair of long bone defects of large size using a tissue-engineered periosteum in a rabbit model. J. Mater. Sci. Mater. Med. 32(9), 105.